Eur. Phys. J. Appl. Phys. (2014) 65: 30301
DOI: 10.1051/epjap/2014130225

THE EUROPEAN PHYSICAL JOURNAL APPLIED PHYSICS

Regular Article

CoO doping effects on the ZnO films through EBPDV technique

Maria Inês Basso Bernardi[1,a], Lauro June Queiroz Maia[2], Eduardo Antonelli[3], Alexandre Mesquita[4], Maximo Siu Li[1], and Lucianna Gama[5]

[1] Instituto de Física de São Carlos, Universidade de São Paulo, PO Box 369, 13560-970 São Carlos, SP, Brazil
[2] Instituto de Física – Universidade Federal de Goiás, Campus II, PO Box 131, 74001-970 Goiânia, GO, Brazil
[3] Instituto de Ciência e Tecnologia, Universidade Federal de São Paulo, 12231-280 São José dos Campos, SP, Brazil
[4] Instituto de Geociências e Ciências Exatas – Universidade Estadual Paulista, 13506-900 Rio Claro, SP, Brazil
[5] Departamento de Engenharia de Materiais – Universidade Federal de Campina Grande, 58109-970 Campina Grande, PB, Brazil

Received: 7 May 2013 / Received in final form: 29 January 2014 / Accepted: 3 February 2014
Published online: 3 March 2014 –

Abstract. Nanometric $Zn_{1-x}Co_xO$ (x = 0.020, 0.025 and 0.030 in mol.%) nanopowders were obtained from low temperature calcination of a resin prepared using the Pechini's method. Firing the $Zn_{1-x}Co_xO$ resin at 400 °C/2 h a powder with hexagonal structure was obtained as measured by X-ray diffraction (XRD). The powder presented average particle size of 40 nm observed by field emission scanning electronic microscopy (FE-SEM) micrographs and average crystallite size of 10 nm calculated from the XRD using Scherrer's equation. Nanocrystalline $Zn_{1-x}Co_xO$ films with good homogeneity and optical quality were obtained with 280–980 nm thicknesses by electron beam physical vapour deposition (EBPVD) under vacuum onto silica substrate at 25 °C. Scanning electron microscopy with field emission gun showed that the film microstructure is composed by spherical grains and some needles. In these conditions of deposition the films presented only hexagonal phase observed by XRD. The UV-visible-NIR and diffuse reflectance properties of the films were measured and the electric properties were calculated using the reflectance and transmittance spectra.

1 Introduction

Semiconductor materials with wide bandgap have attracted much attention nowadays due to the applications in microelectronic and optoelectronic devices [1]. ZnO (zinc oxide) is an well-known n-type semiconductor of wurtzite structure with a direct energy wide bandgap of 3.2–3.3 eV at room temperature [2], and optical transparency in visible range. The resistivity values of ZnO films may be adjusted between 10^{-4} Ω cm and 10^{12} Ω cm by changing the annealing conditions and doping elements [3]. These features have made ZnO applied as transparent electrodes [4], gas sensors [5], solar cell windows [6,7] and photovoltaic devices [8].

ZnO thin films have been prepared by a variety of techniques such as molecular beam epitaxy (MBE) [9], RF magnetron sputtering [10], pulsed laser deposition [11], spray pyrolysis [12], chemical vapor deposition (CVD) [13] and sol-gel processing [14–18]. The sol-gel process is one of the versatile methods to prepare thin film-supported nanosized particles without complicated instruments such as CVD [19]. It is simple, inexpensive and has a general advantage of large area deposition and uniformity of the films thickness [20]. In most cases, the metal alkoxides are used as raw materials for the sol-gel process. But the preparation of a stable sol is tiresome and reagents of metal alkoxides are very costly. Also, diethyl zinc (DEZ) and dimethyl zinc (DMZ) are so reactive that there is a risk of explosion in contact with atmospheric air. Thus, some metal salts, such as nitrates and acetates, are used to change the metal alkoxides for preparing the thin films. Each one of these methods of deposition presents some advantages and/or disadvantages. When the physical methods are used, a source of the material in a crystalline form should be employed to produce the thin films. On the other hand, if a chemical method is used, it is interesting to use very stable, non-toxic and cheaper precursor compounds, like Pechini's method. With this method, we can obtain homogeneous pellets to be used as evaporation source, to prepare thin films in the electron beam physical vapour deposition (EBPVD) technique. Then, for industrial applications, a physical method is required to synthesize thin films.

Much attention has been directed to ZnO doped with transition-metal ions, such as Co ions [21]. This diluted magnetic semiconductor has proposed as an alternative

[a] e-mail: m.basso@if.sc.usp.br

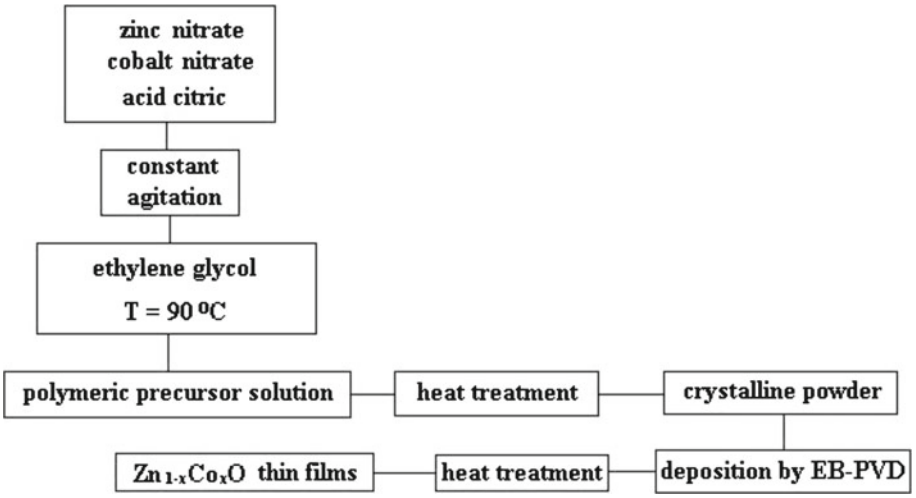

Fig. 1. Flow chart of the $Zn_{1-x}Co_xO$ nanometric synthesis, using a modified Pechini's method.

system for spintronic devices with the advantage of introducing new functionalities that are difficult to be implemented in metallic structures, such as electrical control of both the coercivity [22] and the Curie temperature [23]. Spintronics is a new technology which offers lower switching energies and faster speeds as compared to standard electronics. Such devices are not only novel in terms of lower power requirements and very fast switching speeds, but they also exhibit newer device applications with integrated magnetic, electronic and optical functionality. However, the challenge to implement a commercial spintronic device is to overcome the lack of room-temperature magnetic semiconductor materials that would be used as spin injection layer. Spin injection in semiconductors is a fundamental problem for developing spintronic devices due to the well-known impedance mismatch between semiconductors and ferromagnetic [24]. Despite the huge success achieved in recent years in semiconductor, spintronics is still restricted to cryogenic temperatures. However it has been observed rapid progress toward obtaining materials with magnetic properties that allow the manipulation of spins at room temperature. In the last decade, Dietl et al. reported calculations using the Zener model for the coupling between magnetic ions mediated by free carriers [25]. These authors demonstrated that relatively large gap semiconductors such as GaN and ZnO, could present Curie temperature close to and even superior to room temperature when a fraction of cations of these materials were replaced with ions of transitional metal as Mn or Co [25].

In this work, we report the synthesis of nanometric $Zn_{1-x}Co_xO$ ($x = 0.020$, 0.025 and 0.030 in mol.%) powders using low temperature calcinations of resins prepared by the Pechini's method. Also the production and characterization of nanocrystalline $Zn_{1-x}Co_xO$ thin films by electron beam physical vapour deposition (EBPVD) in vacuum are presented. In order to determine structural properties of the $Zn_{1-x}Co_xO$ powders and films, samples were mainly characterized by optical techniques (transmittance, and diffuse reflectance), scanning electron microscopy with field emission gun (FE-SEM) and X-ray diffraction (XRD).

2 Experimental

2.1 Nanometric $Zn_{1-x}Co_xO$ powders preparation

Details of the nanometric $Zn_{1-x}Co_xO$ powders synthesis used in this study is outlined in the flow chart of Figure 1. The raw materials used for $Zn_{1-x}Co_xO$ were zinc nitrate (99.0% purity, Alfa Aesar), cobalt nitrate (98.0% purity, Aldrich), ethylene glycol (99.9% purity, Synth) and citric acid (99.0% purity, Synth). The resins were formed by dissolution of zinc and cobalt nitrates in a water solution of citric acid (60–70 °C). After homogenization of the solution, ethylene glycol was added to promote polymerization of the mixture by polyesterification reaction.

The molar ratio among the citric acid/metal ratio was fixed at 3:1 and the citric acid/ethylene glycol ratio was fixed at 60:40 (mass ratio). The resin was heated at 120 °C to eliminate excess of water. The heat treatments to obtain the powders were heating of the resin at 400 °C/4 h at 10 °C/min to promote crystallization formation of the desired ZnO phase. Figure 1 illustrates the experimental procedure used.

2.2 Films deposition

$Zn_{1-x}Co_xO$ films deposition was carried out in an electron beam evaporation system (EBPVD), using pellets of the powders as target for evaporation, with a pressure of 4×10^{-6} Torr [26]. The films were obtained with the electron beam gun (Telemark-231) operating at 7 kV and electron beam with 50 mA. Deposition rates of ∼1.0 Å/s were achieved, monitored by a quartz crystal oscillator (Sycon, STM-100). Using this setup we deposited films on silica substrates submitted at 25 °C during the evaporation. The thickness of the films was measured by a Talystep Taylor-Hobson profiler. Tantalum crucibles were used to support

the high temperature achieved during the evaporation of the ZnO pure and cobalt doped pellets. More details of the EBPVD system is described elsewhere [27].

2.3 Microscopy measurements

Scanning electron micrographs (FE-SEM) were taken by a Zeiss (DSM-940A) scanning electron microscope equipped with field emission gun, allowing 100 k× of magnification.

2.4 Structural characterizations of powders and thin films

The crystallinity and phase of the $Zn_{1-x}Co_xO$ powders and films were investigated by XRD technique using a Rigaku Dmax-2500PC diffractometer operating with Cu Kα radiation with 2θ detector scanning ranging from 15 to 75°, in steps of 0.03°. For films was used X-ray grazing angle incidence fixed at 2.0° between the X-ray beam and the film surface, and 2θ detector scanning from 25 to 75°.

2.5 Optical measurements

The UV-visible-NIR spectra of the $Zn_{1-x}Co_xO$ films were collected in transmittance mode in a Cary-17 spectrophotometer, in the 190–1100 nm region. Silica substrates were placed in the reference beam to simultaneously subtract the silica spectra from the films spectra. Diffuse reflectance of the films were measured through a spectrophotometer (Minolta, CM2600d), in the 400–700 nm range, equipped with standard light sources type D65 (day light).

3 Results and discussion

3.1 Nanometric powders characterization

Figure 2 presents the FE-SEM micrograph of the $Zn_{1-x}Co_xO$ powder obtained from the resins calcined at 400 °C/4 h. It is know that powders with nanometric particles are thermodynamically unstable due to the large surface area. It means that the small dimension particles possess high surface energy, leading the $Zn_{1-x}Co_xO$ powder agglomerate. This behavior can be visualized in the FE-SEM micrographs of the ZnO pure and cobalt doped powders presented in Figure 2. Through software analysis of the micrographs the average dimension of these particles was found to be 15–30 nm (ZnO – Fig. 2a) and 10–40 nm ($Zn_{0.970}Co_{0.030}O$ – Fig. 2b).

Figure 3 shows the XRD pattern of the $Zn_{1-x}Co_xO$ powders obtained from the calcination at 400 °C/4 h.

The mean particle sizes were calculated from X-ray line broadening of the (1 0 1) diffraction peak using Scherrer's equation [28]:

$$P_{hkl} = 0.89\lambda/(\beta_{1/2}\cos\theta_{hkl}), \quad (1)$$

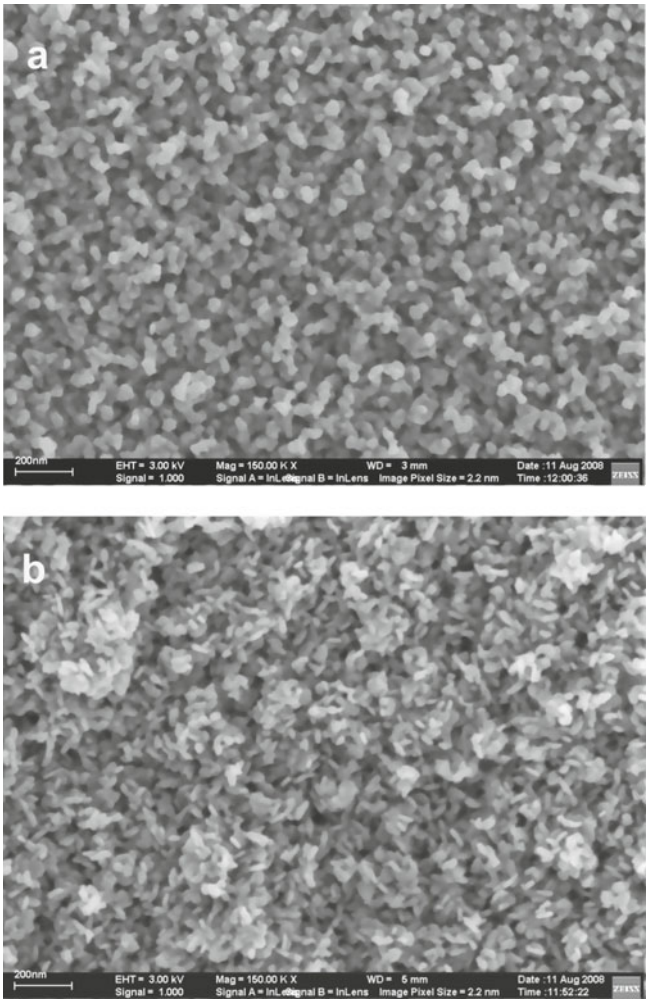

Fig. 2. FE-SEM micrograph of the $Zn_{1-x}Co_xO$ powder obtained from the calcined at 400 °C/4 h: (a) ZnO and (b) $Zn_{0.975}Co_{0.025}O$.

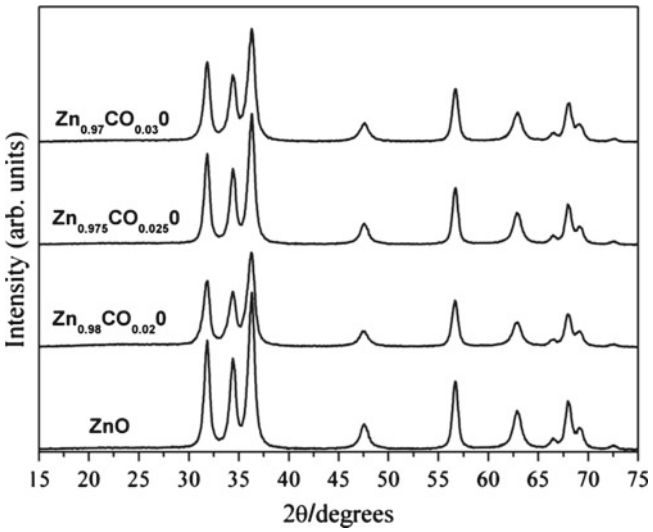

Fig. 3. XRD pattern of the $Zn_{1-x}Co_xO$ powder obtained by Pechini's method, calcined at 400 °C/4 h, index the same phase (JCPDS card No. #36-1451).

where P_{hkl} is the mean crystallite diameter of the particle assumed to be spherical, λ is the radiation wavelength of the X-ray used, θ_{hkl} the diffraction peak angle and $\beta_{1/2}$ is the corrected line width at observed half-peak intensity. The value of $\beta_{1/2}$ was determined from the experimental integral peak width by applying Warren's correction for instrumental broadening [29]; i.e., $\beta^2_{1/2} = \beta^2 - \beta^2_0$, where β_0 is the instrumental broadening determined through the full width at the half maximum (FWHM) of the reflection at 14.2° of SiO_2 powder having particles larger than 1000 Å and β is the FWHM of the (1 0 1) diffraction peak of the sample.

The broad peaks observed in the XRD pattern indicates small average crystallite diameter, which was estimated by the Scherrer's equation as ∼10 nm. It is important to note that the temperature used in this work to obtain the ZnO phase is low compared with conventional ZnO powders, where phase formation and sintering of the particles occurs above 1400 °C [21]. The powders are crystalline at ZnO hexagonal form, indexed by JCPDS card No. #36-1451, independently of CoO addition concentration. Any phase containing cobalt oxide appears in the X-ray patterns shown in Figure 3.

3.2 $Zn_{1-x}Co_xO$ films characterization

Figure 4 shows the XRD pattern of the $Zn_{0.97}Co_{0.30}O$ on silica substrate, obtained after ex-situ heat-treatment at 550 °C/2 h. The peaks that appeared in the pattern were indexed as presenting a hexagonal structure with a $P6_3mc$ space group, which is in agreement with the literature [JCPDS card No. #36-1451]. The film was crystallized randomically, being polycrystalline. There is not a preferred orientation. Almost the same relative intensity between the main peaks ((1 0 0), (0 0 2) and (1 0 1)), we observed for powders and films.

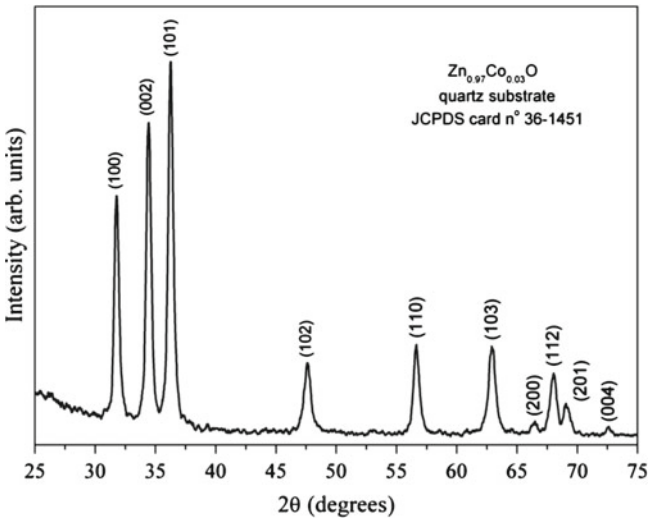

Fig. 4. XRD patterns of $Zn_{0.970}Co_{0.030}O$ films on silica substrate ($P_{101} \sim 17$ nm).

The FE-SEM micrograph presented in Figure 5 shows the film surface morphology. The films are free of cracks and has roughness surface morphology even for different regions analyzed. It is observed that all samples are composed by spherical nanoparticles strongly agglomerated. It was not observed significative morphology change on CoO incorporation. For the sample illustrate in Figure 5a the

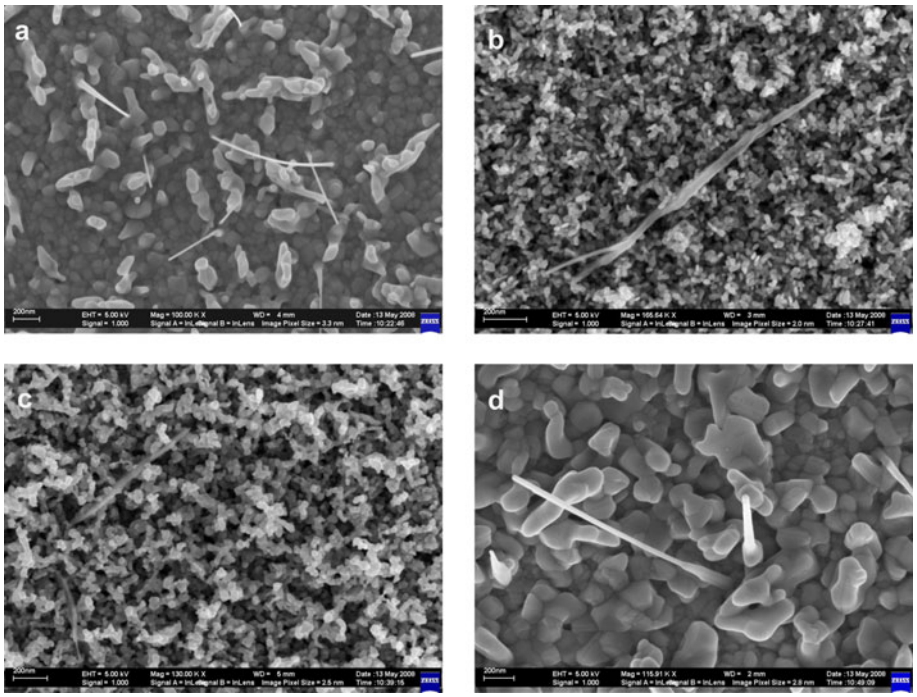

Fig. 5. FE-SEM micrograph of the $Zn_{1-x}Co_xO$ film deposited by EBPVD of the powder obtained by Pechini's method: (a) pure ZnO, (b) $Zn_{0.980}Co_{0.020}O$, (c) $Zn_{0.975}Co_{0.025}O$ and (d) $Zn_{0.0970}Co_{0.030}O$.

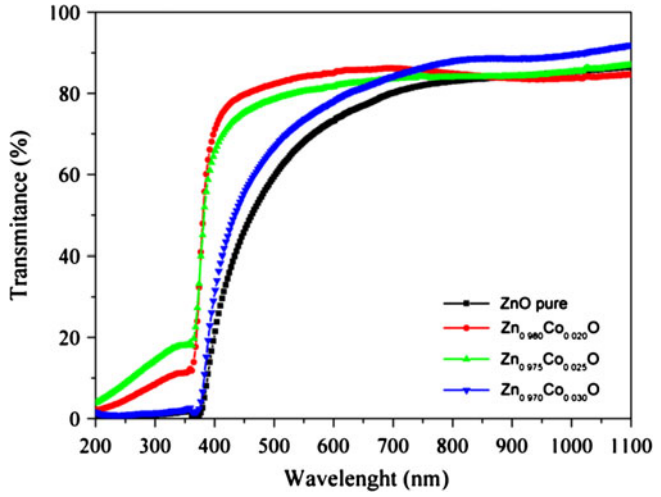

Fig. 6. UV-visible-NIR transmittance of the $Zn_{1-x}Co_xO$ films on silica substrate.

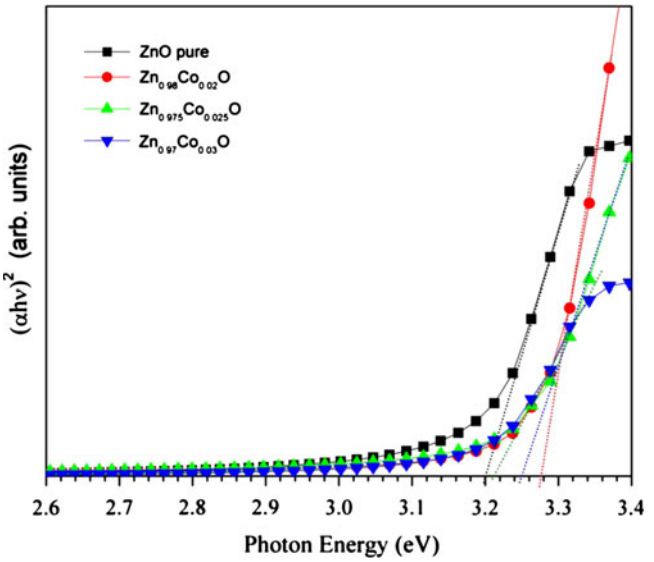

Fig. 7. Absorption coefficient as a function of incident photon energy in the near bandgap region for $Zn_{1-x}Co_xO$ films on silica substrate.

average diameter is 87±10 nm, for Figure 5b is 28±3 nm, for Figure 5c is 36±4 nm and for Figure 5d is 179±19 nm. The films microstructure is not only composed by spherical grains, but also needles with ∼1500 nm-length and ∼50 nm diameter. The needles are initiated on the top of ZnO nanoparticles. The orientation is perpendicular to the surface or randomly tilted, as observed by Falyouni et al. [30]. The growths of these needles do not occur during the EBPVD deposition, but during the ex-situ heat-treatment in electrical furnace at 550 °C. Thus, the needles growth dimensions can be controlled by the furnace temperature and atmosphere. More studies about these needles are required in future works to better understand its growth mechanism, or be the influence of substrate, atmosphere and temperature.

Figure 6 gives the transmittance spectra in the 190–1100 nm region for the films of $Zn_{1-x}Co_xO$ compositions on silica substrate. The 980 nm-thick films has transmittance of 76%, the 280 nm-thick films has transmittance of 86% at 632.8 nm. All films presented good optical quality, with different thicknesses (Tab. 1).

The value of the transmittance used as reference is a direct measure using the He-Ne laser ($\lambda = 632.8$ nm) wavelength. Other optical properties, such as the bandgap and the cut-off, were obtained indirectly. Considering the high absorption region, the transmittance T followed a simple correlation with absorption coefficient [31]:

$$T = B\exp(-\alpha d), \tag{2}$$

where B is approximately equal to the unity at the absorption edge and d is the thickness of the thin films. The relation between the absorption coefficient α and incident photon energy $h\nu$ for allowed direct transition, respectively, can be written as [31,32]:

$$\alpha h\nu = A\left(h\nu - E_g\right)^{1/2}, \tag{3}$$

where A is a constant and E_g is the direct bandgap.

The $(\alpha h\nu)^2$ versus $h\nu$ plots for thin films containing different amounts of CoO and pure are shown in Figure 7. A linear behavior can be observed in a certain range of the curves, supporting the interpretation of direct E_g bandgap for thin films [32]. Therefore, the E_g bandgap of the thin films can be obtained by extrapolating relation (3). Table 1 gives a comparison of the E_g bandgap with the CoO content. As can be seen, the bandgap of thin films increase from 3.17 eV to 3.22 eV as the CoO concentration increase. These values are comparable with those reported by Zou et al. [33].

The diffuse reflectance spectra of $Zn_{1-x}Co_xO$ compounds are presented in Figure 8 have characteristic bands of Co^{2+}, which possess $3d^7$ electronic configuration. There is an absorption band around 550 nm of cobalt in tetrahedral sites (^{2}E), and another band around 510 nm from cobalt in octahedral sites ($^4T_1$) and another at 670 nm. It produces green colored thin films.

Table 1. Transmittance, thickness and optical bandgap (E_g) values with the CoO content in the films.

Films	Substrate	Transmittance (%) at $\lambda = 632.8$ nm	Thickness (±10 nm)	E_g (±0.05 eV)
ZnO pure	Silica	76	920	3.20
$Zn_{0.980}Co_{0.020}O$	Silica	86	280	3.28
$Zn_{0.975}Co_{0.025}O$	Silica	83	300	3.25
$Zn_{0.970}Co_{0.030}O$	Silica	81	980	3.21

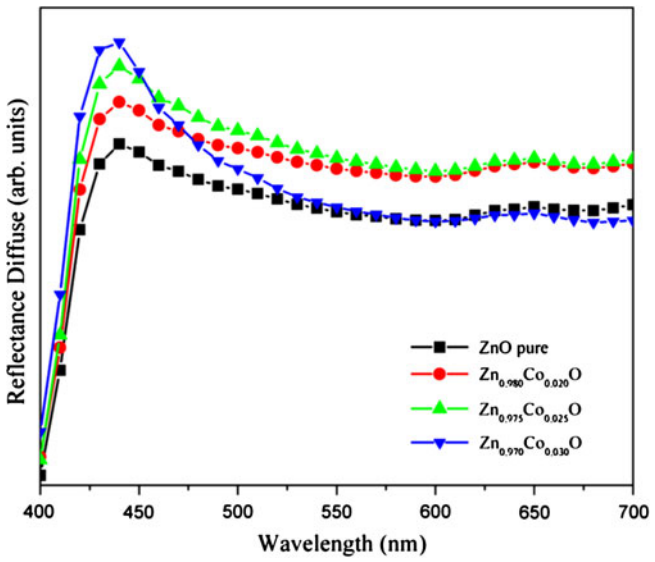

Fig. 8. Reflectance diffuse of the $Zn_{1-x}Co_xO$ films on silica substrate.

The color generation is known by a mechanism named charge transference. This mechanism consist on the electron movement of an ion to another due to the light energy absorption, resulting in a temporary change of the valence state for both ions, originating the material's color [34]. This mechanism is responsible by the color of CoO-doped ZnO compounds. Thus, these synthesized thin films have potential application as attenuators in the visible and near-infrared regions. Also, it can be used as UV filters. Other properties can be explored, like electroluminescence and magneto-optic effects.

Visible spectroscopy (diffuse reflectance) of the powders was performed with a Minolta CM2600d colorimeter in the visible spectrum (Fig. 8). The spectra presented in this paper were used to apply the Kubelka-Munk equation:

$$\text{K-M} = (1-R)^2/2R, \tag{4}$$

where K-M is the Kubelka-Munk function (not shown here), R is the diffuse reflectance from the sample. The optical bandgap, $E_g^{\text{K-M}}$, of the materials were calculated on the basis of the optical spectral absorption using the well-known formula:

$$\text{K-M} = C\left(h\nu - E_g^{\text{K-M}}\right)^{1/2}, \tag{5}$$

where C is a constant and $E_g^{\text{K-M}}$ is the direct bandgap using the Kubelka-Munk function [35].

The $E_g^{\text{K-M}}$ determined values are 2.99 ± 0.05 eV for all powders, independently of the CoO concentration. It shows that the resolution used for collect the diffuse reflectance spectra was not appropriate to identify the CoO effect on the ZnO optical bandgap. Nevertheless, these values are similar to those calculated using the transmission spectra and comparable with the literature [33].

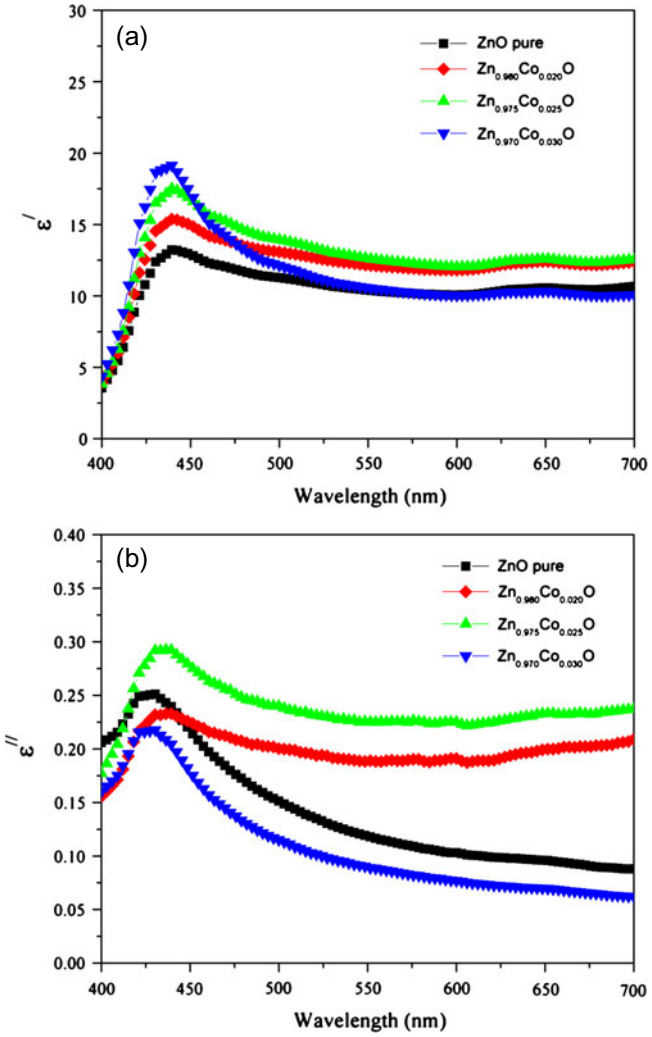

Fig. 9. Variation of real (a) and imaginary (b) of the dielectric constants of the $Zn_{1-x}Co_xO$ films.

The refractive index of the films can be determinate by from the following relation [36]:

$$n = \left[\frac{1+R}{1-R}\right] + \sqrt{\frac{4R}{(1-R)^2} - k^2},$$

where k ($k = \alpha\lambda/4\pi$) is the extinction coefficient that can be directly related to the absorption coefficient (α).

The dielectric constant is defined as, $\varepsilon(\omega) = \varepsilon'(\omega) + i\varepsilon''(\omega)$ and the real and imaginary parts can be determinate by [38]:

$$\varepsilon'(\omega) = n^2(\omega) - k^2(\omega),$$

$$\varepsilon''(\omega) = 2n(\omega)k(\omega).$$

Note that if the medium is only weakly absorbing, k is very small. Thus being the case, these equations show that the refractive index is basically determined by the real part

of the dielectric constant and the absorption is mainly determined by the imaginary part [37].

Figures 9a and 9b present the frequency dependence of the complex electronic dielectric constant. In low wavelength regions (until 475 nm) the electric and magnetic fields are attenuated in amplitude into the material [38]. The reason is that the electrons oscillate out of phase with the electric field. Nevertheless, we can observe that in 440 nm the ε' values increase with increasing of CoO content. It is an indicative of the incorporation of CoO in the ZnO matrix. The same behavior can be described to the imaginary part of the permittivity ε''. When the wavelength is increased (∼475 nm) the behavior of ε' and ε'' can be related with the film microstructure showed in Figure 5. The pure and $x = 0.030$ CoO films present a higher grain size and a smooth surface when compared with the $x = 0.020$ and 0.025 films. It is evident that these characteristics have a great influence on dielectric and optical properties and thus an important parameter to be controlled for applications. The pure and $x = 0.30$ films present a decrease in the ε' and a very pronounced decrease in the ε'', when compared with $x = 0.020$ and $x = 0.25$.

4 Conclusions

In this work we presented the synthesis of nanometric ZnO phases obtained with low temperature calcinations prepared using the Pechini's method. The phase calcining at 400 °C present average particle size from 10 to 40 nm by FE-SEM, and average crystallite size of 10 nm measured by Scherrer equation using the XRD pattern. Transparent, optically smooth and homogeneous $Zn_{1-x}Co_xO$ films with thickness of 280 nm and 980 nm were produced by EBPVD technique, using homogeneous powders obtained by Pechini's method. The films were deposited on silica hold at 25 °C during the evaporation. The synthesized films present hexagonal structure of the ZnO compound with CoO diluted. All films are highly transparent and possess bandgap energy dependent on the CoO addition, and also the transmittance and reflectance spectra. Finally, the ε' and ε'' electrical properties were calculated and show dependence with wavelength and CoO contents.

The authors are grateful to Prof. Dr. Elson Longo and Mr. Rorivaldo Camargo by the FE-SEM measurements and Prof Dr. Fabio Simões de Vicente by important discussion about EBPDV technique. We acknowledge the financial support of the Brazilian research funding institution FAPESP, CAPES and CNPq.

References

1. R. Vinodkumar, I. Navas, K. Porsezian, V. Ganesan, N.V. Unnikrishnan, V.P. Mahadevan Pillai, Spectrochim Acta A **118**, 724 (2014)
2. T. Prakash, R. Jayaprakash, C. Espro, G. Neri, E.R. Kumar, J. Mater. Sci. **49**, 1776 (2014)
3. Z.B. Bahsi, A.Y. Oral, Opt. Mater. **29**, 672 (2007)
4. A. Urbina, J.S. Park, J.M. Lee, S.O. Kim, J.-S. Kim, Nanotechnology **24**, 484013 (2013)
5. S. Devi, V.B. Subrahmanyam, S.C. Gadkari, S.K. Gupta, Anal. Chim. Acta **568**, 41 (2006)
6. R.W. Birkmire, E. Eser, Annu. Rev. Mater. Res. **27**, 625 (1997)
7. W.J. Jeong, S.K. Kim, G.C. Park, Thin Solid Films **506–507**, 180 (2006)
8. G.K.R. Senadeera, K. Nakamura, T. Kitamura, Y. Wada, S. Yanagida, Appl. Phys. Lett. **83**, 5470 (2003)
9. C.J. Pan, C.W. Tu, J.J. Song, G. Cantwell, C.C. Lee, B.J. Pong, G.C. Chi, J. Cryst. Growth **282**, 112 (2005)
10. K.B. Sundaram, A. Khan, Thin Solid Films **295**, 87 (1997)
11. J. Mass, P. Bhattacharya, R.S. Katiyar, Mater. Sci. Eng. B **103**, 9 (2003)
12. P. Nunes, E. Fortunato, R. Martins, Int. J. Inorg. Mater. **3**, 1125 (2001)
13. B.M. Ataev, A.M. Bagamadova, V.V. Mamedov, A.K. Omaev, M.R. Rabadanov, J. Cryst. Growth **198**, 1222 (1999)
14. J. Lee, K. Ko, B. Park, J. Cryst. Growth **247**, 119 (2003)
15. K.L. Narasimhan, S.P. Pai, V.R. Palkar, R. Pinto, Thin Solid Films **295**, 104 (1997)
16. M. Ohayama, H. Kozuka, T. Yoko, Thin Solid Films **306**, 78 (1997)
17. M. Wang, J. Wang, W. Chen, Y. Cui, L. Wang, Mater. Chem. Phys. **97**, 219 (2006)
18. Y. Natsume, H. Sakata, Mater. Chem. Phys. **78**, 170 (2002)
19. F. Peng, H. Wang, H. Yu, S. Chen, Mater. Res. Bull. **41**, 2123 (2006)
20. S. Fujihara, C. Sasaki, T. Kimura, J. Eur. Ceram. Soc. **21**, 2109 (2001)
21. H.B. de Carvalho, M.P.F. de Godoy, R.W.D. Pais, M. Mir, A. Ortiz de Zevallos, F. Iikawa, M.J.S.P. Brasil, V.A. Chitta, W.B. Ferraz, M.A. Boselli, A.C.S. Sabioni, J. Appl. Phys. **108**, 033914 (2010)
22. D. Chiba, M. Yamanouchi, F. Matsukura, H. Ohno, Science **301**, 943 (2003)
23. H. Ohno, D. Chiba, F. Matsukura, T. Omiya, E. Abe, T. Dietl, Y. Ohno, K. Ohtani, Nature **408**, 944 (2000)
24. G. Schmidt, D. Ferrand, L.W. Molenkamp, A.T. Filip, B.J. van Wees, Phys. Rev. B **62**, R4790 (2000)
25. T. Dietl, H. Ohno, F. Matsukura, J. Cibert, D. Ferrand, Science **287**, 1019 (2000)
26. M. Ohring, *Materials Science of Thin Film – Deposition and Structure* (Academic Press, San Diego, 1992)
27. F.S. De Vicente, E.A.A. Rubo, M.S. Li, Rev. Bras. Apl. Vácuo **23**, 11 (2004)
28. P. Sherrer, Göttinger Nachrichten Gesell **2**, 98 (1918)
29. B.E. Warren, *X-Ray Diffraction* (Dover, New York, 1990)
30. F. Falyouni, L. Benmamas, C. Thiandoume, J. Barjon, A. Lusson, P. Galtier, V. Sallet, J. Vac. Sci. Technol. B **27**, 1662 (2009)

31. L.J.Q. Maia, M.I.B. Bernardi, C.A.C. Feitosa, V.R. Mastelaro, A.R. Zanatta, A.C. Hernandes, Thin Solid Films **457**, 246 (2004)
32. C. Terrier, J.P. Chatelon, J.A. Roger, Thin Solid Films **295**, 95 (1997)
33. J. Zou, S. Zhou, C. Xia, X. Zhang, F. Su, G. Peng, X. Li, J. Xu, Thin Solid Films **496**, 205 (2006)
34. H. Colfen, S. Mann, Angew. Chem. Int. Ed. Engl. **42**, 2350 (2003)
35. N. Kislov, S.S. Srinivasan, Y. Emirov, E.K. Stefanakos, Mater. Sci. Eng. B **153**, 70 (2008)
36. M. Caglar, S. Ilican, Y. Caglar, Thin Solid Films **517**, 5023 (2009)
37. M. Fox, *Optical Properties of Solids* (Oxford University Press, Oxford, 2010)
38. J.I. Gersten, F.W. Smith, *The Physics and Chemistry of Materials* (Wiley & Sons, New York, 2001)